Journal of Nano- and Electronic Physics
Vol. **18** No 3, 03010(7pp) (2026)

Журнал нано- та електронної фізики
Том **18** № 3, 03010(7cc) (2026)

OPEN ACCESS

REGULAR ARTICLE

Effect of Bi Doping on the Optical and Structural Properties of ZnO Thin Films: Role of Urbach Energy and Mechanical Stress

S.I. Shulyma[1], N.A. Kurgan[1,*], V.Kh. Kasyanenko[2,1], V.L. Karbivskyy[1], V.V. Stonis[1], N.O. Zueva[1], O.A. Puz'ko[1], L.P. Kliuienko[1], O.I. Sobolev[1]

[1] *G.V. Kurdyumov Institute for Metal Physics NAS of Ukraine, 03142 Kyiv, Ukraine*
[2] *Vinnytsia National Technical University, 21021 Vinnytsia, Ukraine*

(Received 20 February 2026; revised manuscript received 14 June 2026; published online 26 June 2026)

The effect of Bi dopant concentration on the optical and structural properties of ZnO thin films synthesized by radio-frequency magnetron sputtering was investigated, with particular emphasis on Urbach energy and internal mechanical stress. An increase in Bi concentration in ZnO films was found to be accompanied by enhanced mechanical stress, attributed to local lattice distortions. These distortions may arise from the substitution of Zn^{2+} ions by larger Bi^{3+} ions or from the formation of a secondary Bi_2O_3 phase, both of which induce internal stresses development in the films. It was established that at low Bi concentrations (up to 1.8 at. %), mechanical stress does not significantly affect the diameter of the nanocolumns. However, at higher concentrations (> 5 at. %), lateral growth is inhibited, resulting in a reduction in nanocolumn diameter. It was shown that the Urbach energy of Bi-doped ZnO films is significantly higher than that of undoped samples, indicating a broadening of localized states tails due to bismuth doping. Although macroscopic mechanical stress affects the Urbach energy, its non-monotonic dependence on Bi concentration is primarily governed by other factors, particularly local electrostatic potential fluctuations and the disorientation of the nanocolumnar structure.

Keywords: ZnO thin films, Radiofrequency magnetron sputtering, Optical properties, Structural properties, Urbach energy, Mechanical stresses.

DOI: 10.21272/jnep.18(3).03010

PACS numbers: 68.55.J –, 68.37.Hk, 07.85.Jy, 52.70.Gw, 52.70.Kz

1. INTRODUCTION

Zinc oxide (ZnO) is an *n*-type semiconductor with a direct band gap, which is considered as one of the most promising materials for optoelectronic devices [1]. The great interest in ZnO is associated with its high physical and chemical stability [2, 3], low toxicity [1, 4], and low cost (compared to the widely used Indium tin oxide, In_2O_3, SnO_2, and TiO_2) [1, 4], etc. The presence of a wide bandgap (~ 3.36 eV) [5], significant exciton binding energy (60 meV) [5, 6], high transparency in the visible spectral range [7], and significant electronic mobility [8] makes ZnO thin films a promising material for creating photovoltaic elements.

There are various methods for producing ZnO films: metal-organic chemical vapor deposition (MOCVD) [9], sol-gel method [10, 11], chemical vapor deposition (CVD) [12], pulsed laser deposition (PLD) [13], etc. However, only radiofrequency (RF) sputtering magnetron deposition [14] allows obtaining high homogeneity of thin films with good controllability of the film deposition process at a relatively simple and inexpensive production technology.

In recent years, many scientific papers have been devoted to the usage of ZnO-based thin films as an electron transport layer (ETL) in various photovoltaic and optoelectronic devices [15, 16]. However, in order to increase the efficiency of such ZnO-based ETLs, it is necessary to modify them by doping [17, 18], nanostructuring [18-20], etc. [21, 22].

The doping of ZnO films with various elements is one of the most effective and inexpensive methods for improving their properties. However, besides the widely studied ZnO films doped with Al [23-25], Ga [25-27], and In [25, 27], the optical and structural properties of ZnO films modified with bismuth (Bi) remain insufficiently investigated.

The Bi doping has attracted researchers' considerable attention due to the possibility of improving the optical and electrical properties of ZnO [28, 29]. The bismuth addition to ZnO can change the crystal structure [29] of the material, alter the band gap [28, 30], and improve the optical properties [30]. This opens up new prospects for ZnO:Bi films usage as ETL layers in photovoltaic and optoelectronic devices. However, the data on the change in the parameters of such films are quite controversial [28, 30] and need to be verified and clarified.

This paper presents a study of the effect of Bi concentration on the optical (absorption, Urbach energy) and structural (mechanical stress) properties of ZnO thin films deposited by RF magnetron sputtering onto glass substrates. These results are important for optimizing ZnO:Bi films for use as electron transport layers (ETLs) in solar cells, as well as in sensors and optoelectronic devices [31-33].

* Correspondence e-mail: kurgan@imp.kiev.ua

Cite this article as: S.I. Shulyma et al., *J. Nano- Electron. Phys.* 18 No 3, 03010 (2026) https://doi.org/10.21272/jnep.18(3).03010

2. EXPERIMENTAL DETAILS

ZnO thin films with varying Bi dopant concentrations were deposited by RF magnetron sputtering (13.56 ± 0.135 MHz) from a circular target with an area of ~ 12.5 cm^2. The initial powders of ZnO (LLC "Khimlaborreaktiv", purity ≥ 99.9 %) and Bi_2O_3 (LLC "Reakhim", purity ≥ 99.5 %) were blended in weight ratios of 95:5 (BZO1), 85:15 (BZO2), and 80:20 (BZO3). These mixtures were pressed into discs with a diameter of 4.0 cm and employed as sputtering targets, which were subsequently mounted in the chamber of a universal vacuum system (VUP-5M) for film deposition.

The films were deposited onto glass substrates (1 × 1 cm^2). Prior to deposition, the substrates were ultrasonically cleaned in isopropyl alcohol (40 kHz, 20 min) and then rinsed with deionized water. The target-to-substrate distance was maintained at 4.5 ± 0.1 cm.

Prior to deposition, a base pressure of 5.0×10^{-5} Pa was established in the VUP-5M vacuum chamber using a fore-vacuum pump and a diffusion pump with a cryogenic nitrogen condensation trap. Argon (purity 99.9 %) was used as the working gas. The deposition pressure in the chamber was maintained at 1 Pa. The sputtering power and deposition time were set to 120 W and 60 min, respectively. Deposition was carried out without substrate heating.

The crystal structure was analyzed by X-ray diffraction (XRD) using a Shimadzu LabX XRD-6000 diffractometer (X-ray tube power: 35kV/30mA) with Cu Kα radiation (λ = 1.5406 Å) in Bragg–Brentano geometry (scanning step Δ(2θ): 0.02°, 2θ range: 29°-70°, accumulation time: 1 s).

Morphological analysis of ZnO, BZO1, BZO2, and BZO3 thin films was performed using scanning electron microscopy (SEM) on a Tescan Mira 3 microscope with an accelerating voltage of 5-20 kV. Energy-dispersive X-ray (EDX) analyses were performed using the built-in Oxford X-max 80 mm^2 detector.

Spectrophotometric measurements were performed using a Spekol 1500 single-beam spectrophotometer in the 300-1100 nm spectral range with a scanning step of 1 nm. Slide glass was used as the reference for optical absorption measurements.

3. RESULTS AND DISCUSSION

The elemental composition of ZnO, BZO1, BZO2, and BZO3 thin films was analyzed by EDX (Fig. 1). It was found that with increasing Bi concentration (φ_{Bi}) in the ZnO:Bi films, the Zn content decreases, while the oxygen content increases.

This behavior can be attributed to the substitution of Zn^{2+} ions by larger Bi^{3+} ions in the lattice, the possible formation of interstitial defects, and the emergence of a secondary Bi_2O_3 phase, all of which contribute to the development of internal mechanical stress. Due to the higher valence of Bi^{3+} and its significantly larger ionic radius (r_{ion} = 1.03 Å [34]) compared to Zn^{2+} (r_{ion} = 0.60 Å [35]), Bi incorporation induces local lattice distortions and stress in ZnO:Bi thin films. The simultaneous increase in oxygen content suggests activation of charge-compensation mechanisms, including the incorporation of excess oxygen, a reduction in oxygen vacancy (V_o) concentration, and the formation of Bi-O complexes.

At high Bi concentrations (BZO2 and BZO3 samples), an increase in the O/(Zn+Bi) ratio is observed, which may indicate partial phase separation accompanied by the formation of nanoscale Bi_2O_3 inclusions. A similar effect, specifically the formation of a δ-Bi_2O_3 phase within the films, was reported in our previous study [36].

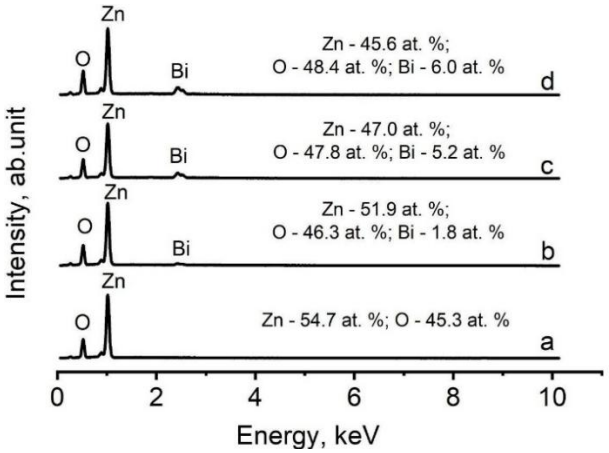

Fig. 1 – EDX spectra of thin films: a) ZnO; b) BZO1; c) BZO2; d) BZO3

Cross-sectional images of thin films obtained by SEM were used to analyze the internal structure and determine the thickness of the films (Fig. 2). The ZnO, BZO1, BZO2, and BZO3 films consist of a nanocolumnar structure, characteristic of columnar crystal growth.

As previously reported [36], the nanocolumns in undoped ZnO films are predominantly oriented along the [002] direction, as evidenced by a single intense (002) XRD peak (Fig. 3a). For BZO1 films, a slight misorientation of the nanocolumnar structure relative to the [002] axis is observed (Fig. 2b), which can be attributed to the presence of a small fraction of ZnO crystallites oriented along the [012] and [013] directions. This interpretation is supported by the appearance of the corresponding (012) and (013) XRD peaks on Fig. 3b.

Low Bi doping (up to 1.8 at. %, sample BZO1) has little effect on the average nanocolumn diameter, which remains 17-20 nm for both ZnO and BZO1 films. However, increasing the Bi concentration to 5.2 at. % and 6.0 at. % (BZO2 and BZO3) significantly suppresses lateral growth, resulting in a reduction of the average nanocolumn diameter to ~ 8 nm and ~ 5 nm, respectively.

XRD patterns of ZnO, BZO1, BZO2, and BZO3 thin films were obtained to determine the lattice parameters and confirm phase formation (Fig. 3). The position of the (002) diffraction peak (2θ = 34.43°) for undoped ZnO thin films coincides with powder sample ZnO (JCPDS card No. 96-230-0451) with hexagonal wurtzite structure. The lattice parameters a and c were determined from the XRD data using a biaxial stress model [37], assuming zero stress perpendicular to the film surface (σ_z = 0), which is typical for thin films ZnO and consistent with literature reports [37, 38].

For the ZnO:Bi samples, the positions of the (100) and (101) diffraction peaks were used to determine the lattice parameters a and c. The detailed procedure and calculated values are reported in [36] and summarized in Table 1.

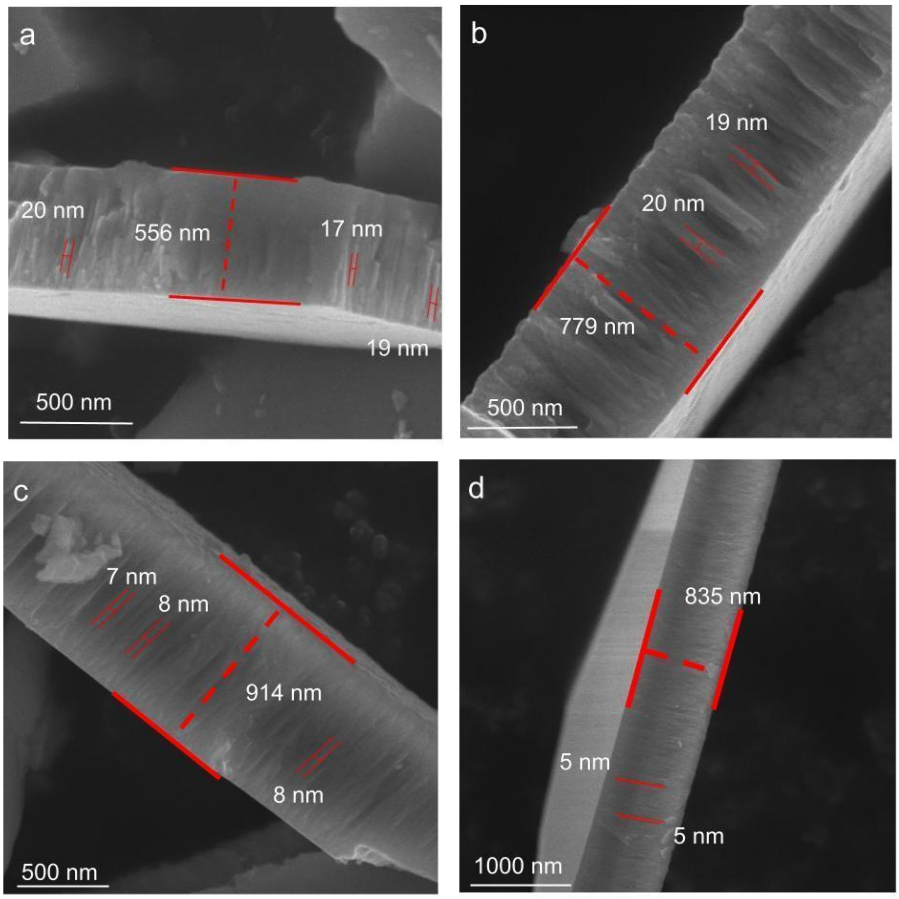

Fig. 2 – SEM images of thin films cross-sections: a) ZnO; b) BZO1; c) BZO2; d)BZO3

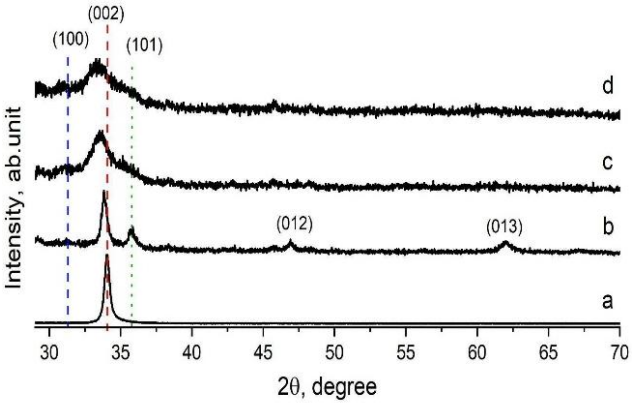

Fig. 3 – XRD patterns of the films: a) ZnO; b) BZO1; c) BZO2; d) BZO3 [36]

Optical absorption spectra were obtained to determine the effect of Bi concentration on the optical properties of ZnO thin films (Fig. 4a). Bi doping was found to increase the optical absorption of the ZnO films.

This behavior may be attributed to both an increase in film thickness (Fig. 2) and the emergence of additional structural inhomogeneities, including structural disorder, internal mechanical stress, and surface effects that enhance optical scattering etc. To evaluate the influence of these factors, the Urbach energy was determined for ZnO, BZO1, BZO2, and BZO3 thin films (Fig. 4b).

Any deviation from the ideal crystal structure leads to modifications of the electronic band structure. Therefore, analysis of optical absorption in the spectral region corresponding to the band-tail states enables determination of the Urbach energy (E_U) and, consequently, assessment of the degree of structural disorder in the material.

It should be noted that, in addition to structural disorder, the Urbach energy includes a contribution associated with thermal lattice vibrations [39], which increases with temperature. At room temperature ($T = 300$ K), the thermal energy is approximately $kT \approx 26$ meV. Since all measurements were performed at the same temperature ($T = 300$ K), this component can be considered constant and does not affect the comparative analysis of E_U among the studied samples.

The Urbach energy E_U was determined from the slope of the linear region of the $\ln(\alpha)$ versus photon energy ($h\upsilon$) plot (Fig. 4b):

$$\ln(\alpha) = \frac{h\upsilon}{E_U} + constant \qquad (1)$$

The corresponding Urbach energy values for ZnO, BZO1, BZO2, and BZO3 films are presented in Table 1 and Fig. 5. The error in determining the Urbach energy was 3 meV.

Table 1 – Urbach energy and structural parameters of ZnO, BZO1, BZO2, and BZO3 thin films

	φ_{Bi}, at.%	a, Å	c, Å	E_U, meV	$(c - c_0)/c_0$, $\times 10^{-3}$	$\sigma_\perp$, $\times 10^9$ N·m^{-2}	$(a - a_0)/a_0$, $\times 10^{-3}$	$\sigma_\parallel$, $\times 10^9$ N·m^{-2}
ZnO	0	3.250 ± 0.001 [36]	5.210 ± 0.001 [36]	136 ± 3	–	–	–	–
BZO1	1.8	3.252 ± 0.001 [36]	5.239 ± 0.001 [36]	291 ± 3	5.64 ± 0.01	1.36 ± 0.01	0.83 ± 0.01	0.87 ± 0.01
BZO2	5.2	3.279 ± 0.001 [36]	5.286 ± 0.001 [36]	243 ± 3	14.59 ± 0.01	4.96 ± 0.01	9.02 ± 0.01	4.51 ± 0.01
BZO3	6.0	3.287 ± 0.001 [36]	5.309 ± 0.001 [36]	278 ± 3	18.96 ± 0.01	6.40 ± 0.01	11.51 ± 0.01	5.79 ± 0.01

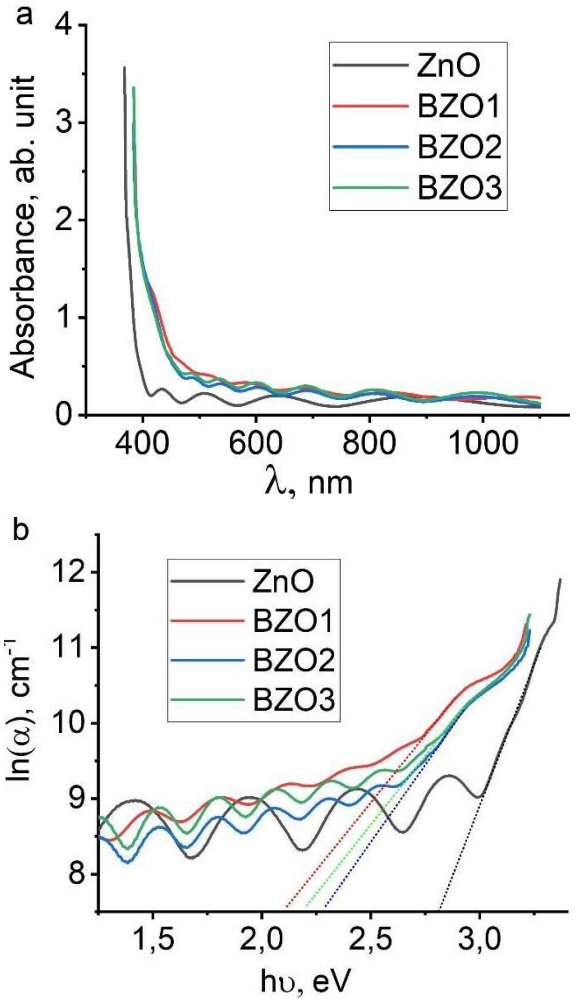

Fig. 4 – Optical properties of ZnO, BZO1, BZO2, and BZO3 thin films: a) optical absorption spectra; b) Urbach energy determination. λ – wavelength; α – optical absorption coefficient

For a hexagonal crystal structure, the stress tensor can be expressed as follows [38]:

$$\begin{Bmatrix}\sigma_x\\ \sigma_y\\ \sigma_z\end{Bmatrix} = \begin{Bmatrix}C_{11} & C_{12} & C_{13}\\ C_{12} & C_{11} & C_{13}\\ C_{13} & C_{13} & C_{33}\end{Bmatrix}\begin{Bmatrix}\varepsilon_{xx}\\ \varepsilon_{yy}\\ \varepsilon_{zz}\end{Bmatrix} \quad (2)$$

where C_{ij} are the elastic stiffness constants and ε_{ii} are the linear strains in the i-th direction.

The linear strain normal to the substrate surface (ε_{zz}) is given by $\varepsilon_{zz} = \varepsilon_c = (c - c_0)/c_0$, where c_0 and c are the lattice parameters of undoped ZnO and Bi-doped ZnO thin films, respectively. Due to the in-plane isotropy of the hexagonal structure, the in-plane strains are equal and can be expressed as $\varepsilon_{xx} = \varepsilon_{yy} = \varepsilon_a = (a - a_0)/a_0$, where a_0 and a are the in-plane lattice parameters of undoped and Bi-doped ZnO films, respectively.

Taking the above into account, Eq. (2) yields the following expressions for the BZO1, BZO2 and BZO3 films:

$$\begin{cases}\sigma_\parallel = (C_{11} + C_{12})\varepsilon_a + C_{13}\varepsilon_c\\ \sigma_\perp = 2C_{13}\varepsilon_a + C_{33}\varepsilon_c\end{cases} \quad (3)$$

where $\sigma_\parallel = \sigma_x = \sigma_y$ is the in-plane stress, $\sigma_\perp = \sigma_z$ is the normal to the film surface stress (hereafter, normal stress), and elastic stiffness constants for ZnO are $C_{11} = C_{33} = 2.1 \times 10^{11}$ N·m^{-2}, $C_{12} = 1.2 \times 10^{11}$ N·m^{-2}, $C_{13} = 1.05 \times 10^{11}$ N·m^{-2} [37].

The calculated values of the in-plane and normal stresses are presented in Table 1 and Fig. 5. The higher Urbach energy values observed in ZnO:Bi thin films compared to undoped ZnO (Fig. 5) may be attributed to increased structural and electronic disorder caused by the size and charge mismatch between Bi and Zn ions, the formation of defects and internal mechanical stress, structural disorientation, and the possible formation of Bi-enriched regions. These factors lead to a broadening of the band-tail states in the bandgap.

For single-crystal ZnO films, the Urbach energy typically ranges from 74 to 99 meV [40]. In contrast, the higher experimentally determined value of $E_U = 136 \pm 3$ eV for undoped ZnO thin films indicates the presence of structural disorder and band-tail states associated with intrinsic defects.

Compared to undoped ZnO, the Urbach energy (E_U) of ZnO:Bi thin films increases significantly, reaching 243 ± 3 to 291 ± 3 meV (Table 1). This behavior can be attributed to: (i) the pronounced size and charge mismatch between Bi^{3+} and Zn^{2+} ions, leading to local lattice distortions, internal mechanical stress, and fluctuations in interatomic distances; (ii) the formation of defects (e.g., excess oxygen) and Bi–O complexes in the film (the appearance of δ-Bi_2O_3 inclusions was shown in [36]); and (iii) local electrostatic potential fluctuations arising from these structural perturbations.

At low Bi concentrations (BZO1 samples, $\varphi_{Bi} \approx 1.8$ at. %), the Bi^{3+} ions are sparsely and predominantly randomly distributed within the film. This leads to the formation of point defects (Bi_{Zn}, V_{Zn}, O_i), accompanied by local potential fluctuations and internal mechanical stress. However, the magnitude of these stresses does not play a dominant role in determining the Urbach energy at this Bi doping level of ZnO:Bi thin

films. In particular, the in-plane stress ($\sigma_{\parallel} \approx (0.87 \pm 0.01) \times 10^9$ N·m^{-2}) is insufficient to destroy the nanocolumnar structure characteristic of undoped ZnO films (Fig. 2). Consequently, the average nanocolumn diameter remains nearly unchanged (~ 18-20 nm) for both ZnO and BZO1 films.

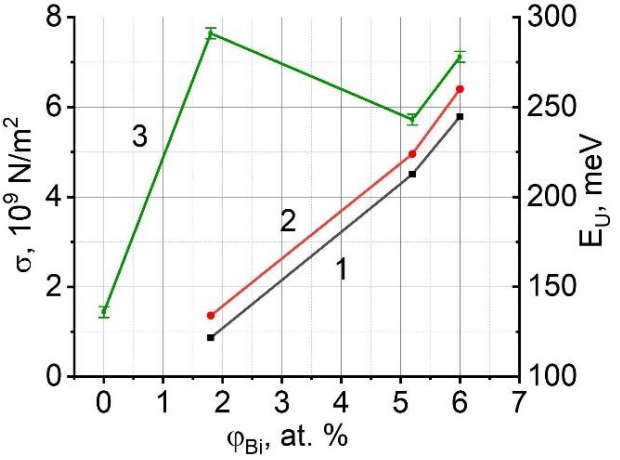

Fig. 5 – Dependence in-plane stress ($\sigma_{\parallel}$) – curve 1, normal stress ($\sigma_{\perp}$) – curve 2, and Urbach energy (E_U) – curve 3 on Bi concentration (φ_{Bi}) in ZnO:Bi films

XRD patterns analysis of BZO1 thin films (Fig. 3b) reveals the appearance of additional reflections (100), (101), (012), and (013) compared to undoped ZnO films. Furthermore, SEM analysis shows a slight misorientation of the nanocolumnar structure in BZO1 thin films relative to the [002] direction (Fig. 2b), indicating a deviation from the predominant *c*-axis growth and an increase in structural disorder. This misorientation correlates with higher Urbach energy values compared to BZO2 and BZO3 films, in which such effects are not observed.

At higher Bi concentrations ($\varphi_{Bi} > 5$ at. %, BZO2 and BZO3), an increase in both in-plane and out-of-plane stresses is observed (Table 1 and Fig. 5). Under these conditions, crystallite growth occurs predominantly perpendicular to the film surface, consistent with SEM results for the BZO2 and BZO3 samples (Fig. 2c,d). This is further supported by the disappearance of the (012) and (013) reflections and the partial merging of the (101) peak with the intense (002) reflection upon increasing Bi concentration (Fig. 3c,d), indicating a strengthening of the preferred growth orientation.

A significant increase in in-plane stress ($\sigma_{\parallel} > 4.5 \times 10^9$ N·m^{-2}) at Bi concentrations of 5.2 at.% and 6.0 at.% (Table 1 and Fig. 5) leads to suppression of lateral nanocolumn growth and a substantial reduction in their diameter to ~ 8 nm and ~ 5 nm, respectively (Fig. 2c,d).

Despite a significant increase in both normal ($\sigma_{\perp}$) and in-plane ($\sigma_{\parallel}$) stresses in BZO2 and BZO3 thin films compared to BZO1 samples (Fig. 5), the Urbach energy values are lower for these samples. This observation further indicates that internal mechanical stress does not play a decisive role in determining the Urbach energy in ZnO:Bi thin films. The reduction in Urbach energy for BZO2 and BZO3 samples relative to BZO1 thin films may be attributed to a decrease in local electrostatic potential fluctuations with increasing φ_{Bi} in ZnO:Bi thin films. This results in a lower contrast of local potential fluctuations within the film volume.

Furthermore, XRD patterns (Fig. 3b) indicate that BZO1 films exhibit a higher degree of the nanocolumnar structure disorder, as evidenced by the presence of crystallites oriented along the [012] and [013] directions. Such crystallite misorientation also contributes to an increase in the Urbach energy.

Despite the monotonic increase in both $\sigma_{\parallel}$ and $\sigma_{\perp}$ with increasing Bi concentration in ZnO:Bi films, the Urbach energy exhibits a non-monotonic behavior. In particular, BZO2 and BZO3 samples show lower Urbach energy values than BZO1, despite significantly higher stress levels (Table 1, Fig. 5). This indicates that the formation of band-tail states in ZnO:Bi thin films is governed not by average macroscopic stress, but rather by factors such as local electrostatic potential fluctuations and nanocolumnar structural disorder.

The results demonstrate that the optical properties (notably optical absorption and Urbach energy) and structural characteristics of ZnO:Bi thin films – including nanocolumn diameter and internal mechanical stress – are strongly dependent on Bi dopant concentration. The non-monotonic dependence of the Urbach energy reflects a complex interaction between structural and electronic disorder. These findings highlight the usefulness of the Urbach energy as a sensitive indicator of film quality and structural-electronic disorder, which is important for optimizing ZnO:Bi thin films for potential applications in photocatalysis, sensing, and optoelectronic devices.

4. CONCLUSIONS

This study investigated the effect of Bi dopant concentration on the optical and structural properties of ZnO:Bi thin films synthesized by radiofrequency magnetron sputtering, with particular emphasis on Urbach energy and internal mechanical stresses.

An increase in Bi concentration (φ_{Bi}) in ZnO:Bi thin films is accompanied by a rise in internal mechanical stress, attributed to local lattice distortions caused by the substitution of Zn^{2+} ions with larger Bi^{3+} ions and/or the formation of a secondary Bi_2O_3 phase. The lattice parameters (*a* and *c*) of the hexagonal wurtzite structure, as well as the in-plane ($\sigma_{\parallel}$) and out-of-plane ($\sigma_{\perp}$) stresses, increase with increasing φ_{Bi}.

At low Bi doping levels ($\varphi_{Bi} \sim 1.8$ at. %), the in-plane stress ($\sigma_{\parallel} \approx (0.87 \pm 0.01) \times 10^9$ N·m^{-2}) is insufficient to destroy the nanocolumnar structure characteristic of undoped ZnO films, and the average nanocolumn diameter remains ~ 18-20 nm. At higher Bi concentrations (5.2 and 6.0 at.%), significantly increased in-plane stress ($\sigma_{\parallel} \approx (4.51 \pm 0.01) \times 10^9$ and $(5.79 \pm 0.01) \times 10^9$ N·m^{-2}, respectively) suppresses lateral nanocolumn growth, resulting in a considerable reduction in average nanocolumn diameter to ~ 8 nm and ~ 5 nm.

It was found that Bi doping leads to a substantial increase in the Urbach energy, from $E_U = 136 \pm 3$ meV for undoped ZnO thin films to $E_U = 243 \pm 3 - 291 \pm 3$ meV for ZnO:Bi films, indicating enhanced structural and electronic disorder and a broadening of band-tail states.

The Urbach energy exhibits a non-monotonic dependence on Bi concentration, reaching a maximum

value of 291 ± 3 meV at $\varphi_{Bi} = 1.8$ at. %, followed by a decrease to 243 ± 3 meV and 278 ± 3 meV at $\varphi_{Bi} = 5.2$ and $\varphi_{Bi} = 6.0$ at. %, respectively. Although macroscopic mechanical stress contributes to E_U in ZnO:Bi thin films, this non-monotonic behavior is primarily governed by local electrostatic potential fluctuations and nanocolumnar structural misorientation rather than by averaged stresses within the film.

FUNDING

The work was financially supported by the National Academy of Sciences of Ukraine in the framework of the Project No 3-A (0125U000325).

DECLARATION OF COMPETING INTEREST

The authors declare that they have no known competing financial interests or personal relationships that could have appeared to influence the work reported in this paper.

DATA AVAILABILITY

Data will be made available on request.

AUTHORSHIP CONTRIBUTION STATEMENT

S.I. Shulyma: Writing – review & editing, Writing – original draft, Methodology, Investigation, Formal analysis, Supervision, Conceptualization. **N.A. Kurgan:** Writing – review & editing, Writing – original draft, Visualization, Investigation. **V.Kh. Kasyanenko:** Formal analysis. **V.L. Karbivskyy:** Supervision, Project administration, Funding acquisition. **V.V. Stonis:** Investigation. **N.O. Zueva:** Visualization, Investigation. **O.A. Puz`ko:** Visualization, Investigation. **L.P. Kliuienko:** Investigation. **O.I. Sobolev:** Investigation.

REFERENCES

1. Ü. Özgür, Ya.I. Alivov, C. Liu, A. Teke, M.A. Reshchikov, S. Doğan, V. Avrutin, S.-j. Cho, H. Morkoç, *J. Appl. Phys.* **98**, 041301 (2005) https://dx.doi.org/10.1063/1.1992666.
2. D. Segets, J. Gradl, R.K. Taylor, V. Vassilev, W. Peukert, *ACS Nano* **3** No 7, 1703 (2009) https://doi.org/10.1021/nn900223b.
3. X. Luo, Z. Lou, L. Wang, X. Zheng, T. Zhang, *New J. Chem.* **38**, 84 (2013) https://doi.org/10.1039/C3NJ00776F.
4. A. Kołodziejczak-Radzimska, T. Jesionowski, *Materials* **7** No 4, 2833 (2014) https://doi.org/10.3390/ma7042833.
5. D. Banerjee, J.Y. Lao, D.Z. Wang, J.Y. Huang, Z.F. Ren, D. Steeves, B. Kimball, M. Sennett, *Appl. Phys. Lett.* **83**, 2061 (2003) https://dx.doi.org/10.1063/1.1609036.
6. D.G. Thomas, *J. Phys. Chem. Solids* **15** No 1-2, 86 (1960) https://doi.org/10.1016/0022-3697(60)90104-9.
7. Mursal, Irhamni, Bukhari, Z. Jalil, *J. Phys.: Conf. Ser.* **1116**, 032020 (2018) (https://dx.doi.org/10.1088/1742-6596/1116/3/032020.
8. N.A. Jayah, H. Yahaya, M.R. Mahmood, T. Terasako, K. Yasui, A.M. Hashim, *Nanoscale Res. Lett.* **10**, 7 (2015) https://doi.org/10.1186/s11671-014-0715-0.
9. N.M. Sbrockey, S. Ganesan, *III-Vs Rev.* **17** No 7, 23 (2004) https://doi.org/10.1016/S0961-1290(04)00735-5.
10. J.N. Hasnidawani, H.N. Azlina, H. Norita, N.N. Bonnia, S. Ratim, E.S. Ali, *Procedia Chem.* **19**, 211 (2016) https://doi.org/10.1016/j.proche.2016.03.095.
11. S.A. Kamaruddin, K.-Y. Chan, H.-K. Yow, M.Z. Sahdan, H. Saim, D. Knipp, *Appl. Phys. A Mater. Sci. Process.* **104**, 263 (2010) https://doi.org/10.1007/s00339-010-6121-2.
12. J. Hu, R.G. Gordon, *J. Appl. Phys.* **71**, 880 (1992) https://dx.doi.org/10.1063/1.351309.
13. Y.Y. Villanueva, D.-R. Liu, P.T. Cheng, *Thin Solid Films* **501** No 1-2, 366 (2005) https://doi.org/10.1016/j.tsf.2005.07.152.
14. S.H. Jeong, S. Kho, D. Jung, S.B. Lee, J.-h. Boo, *Surf. Coat. Technol.* **174–175**, 187 (2003) https://doi.org/10.1016/S0257-8972(03)00600-5.
15. C. Qiu, Y. Wu, J. Song, W. Wang, Z. Li, *Coatings* **12** No 12, 1981 (2022) https://doi.org/10.3390/coatings12121981.
16. D.C. Tiwari, S.K. Dwivedi, P. Dipak, T. Chandel, R. Sharma, *AIP Conf. Proc.* **1832** No 1, 060024 (2017) https://dx.doi.org/10.1063/1.4980429.
17. X. Liu, Y. Ji, Z. Xia, D. Zhang, Y. Cheng, X. Liu, X. Ren, X. Liu, H. Huang, Y. Zhu, X. Yang, X. Liao, L. Ren, W. Tan, Z. Jiang, J. Lu, C. McNeill, W. Huang, *Adv. Sci.* **11** No 37, 2402158 (2024) https://doi.org/10.1002/advs.202402158.
18. N.A.Z. Abidin, F. Arith, N.S. Noorasid, H. Sarkawi, A.N. Mustafa, N.E. Safie, A.S.M. Shah, M.A. Azam, P. Chelvanathan, N. Amin, *RSC Adv.* **13** No 48, 33797 (2023) https://doi.org/10.1039/D3RA04823C.
19. G. Bagha, K. Samavati, H. Naffakh-Moosavy, L.F. Matin, *Sci Rep.* **14**, 4617 (2024) https://doi.org/10.1038/s41598-024-55379-w.
20. W.B. Tarique, M.H. Rahaman, S.S. Dipta, A.H. Howlader, A. Uddin, *Nanomanufacturing* **4**, 81 (2024) https://doi.org/10.3390/nanomanufacturing4020006.
21. F. Eisner, A. Seitkhan, Y. Han, D. Khim, E. Yengel, A.R. Kirmani, J. Xu, F.P.G. De Arquer, E.H. Sargent, A. Amassian, Z. Fei, M. Heeney, T.D. Anthopoulos, *Sol. RRL* **2** No 3, 1800076 (2018) https://doi.org/10.1002/solr.201800076.
22. J. Ma, Z. Lin, X. Guo, J. He, Z. Hu, J. Su, J. Zhang, J. Chang, Y. Hao, *Mater. Today Energy* **14**, 100351 (2019) https://doi.org/10.1016/j.mtener.2019.100351.
23. A.I. Kashuba, B. Andriyevsky, H.A. Ilchuk, R.Yu. Petrus, T.S. Malyi, I.V. Semkiv, *J. Nano- Electron. Phys.* **13** No 4, 04006 (2021) https://doi.org/10.21272/jnep.13(4).04006.
24. V.V. Zaika, N.K. Shvachko, V.H. Kasiyanenko, V.L. Karbivskyy, V.O. Moskaliuk, I.V. Sukhenko, A.P. Soroka, *Funct. Mater.* **31** No 2, 185 (2024) https://dx.doi.org/10.15407/fm31.02.185.
25. P. Nunes, E. Fortunato, P. Tonello, F. Braz Fernandes, P. Vilarinho, R. Martins, *Vacuum* **64** No 3-4, 281 (2002) https://doi.org/10.1016/S0042-207X(01)00322-0.
26. S.D. Ponja, S. Sathasivam, I.P. Parkin, C.J. Carmalt, *Sci. Rep.* **10**, 638 (2020) https://doi.org/10.1038/s41598-020-57532-7.
27. S.I. Shulyma, I.V. Sukhenko, V.K. Kasyanenko, V.L. Karbivskyy, N.A. Kurgan, N.K. Shvachko, V.V. Zaika, V.O. Moskaliuk, O.A. Puzko, *Ukr. J. Phys.* **70** No 9, 609 (2025) https://doi.org/10.15407/ujpe70.9.609.
28. C. Sermsrithong, P. Jaidaew, C. Promjantuk, P. Buabthong, *Int. J. Eng. Trans. C: Aspects* **35** No 12, 2344 (2022) https://doi.org/10.5829/ije.2022.35.12c.10.
29. P. Krongarrom, S.T. Rattanachan, T. Fangsuwannarak, *Eng. J.* **16** No 3, 59 (2012) https://doi.org/10.4186/ej.2012.16.3.59.
30. F. Chouikh, Y. Beggah, M.S. Aida, *J. Mater. Sci: Mater. Electron.* **22**, 499 (2010) https://doi.org/10.1007/s10854-010-0167-y.
31. S.S. Zahirullah, P. Immanuel, S. Pravinraj, P.F.H. Inbaraj, J.J. Prince, *Mater. Lett.* **230**, 1 (2018) https://doi.org/10.1016/j.matlet.2018.07.067.
32. J. Naidoo, T. Fangsuwannarak, S. Laohawiroj, P. Rattana-

wichai, W. Limsiri, R. Phatthanakun, *Integr. Ferroelectr.* **225** No 1, 124 (2022) https://doi.org/10.1080/10584587.2022.2054062.
33. M. Jiang, X. Liu, H. Wang, *Surf. Coat. Technol.* **203** No 24, 3750 (2009) https://doi.org/10.1016/j.surfcoat.2009.06.014.
34. H. Li, P.J. Sadler, H. Sun, *J. Biol. Chem.* **271** No 16, 9483 (1996) https://doi.org/10.1074/jbc.271.16.9483.
35. R.D. Shannon, C.T. Prewitt, *Acta Crystallogr. Sect. B* **25**, 925 (1969) https://doi.org/10.1107/S0567740869003220.
36. S.I. Shulyma, N.A. Kurgan, V.L. Karbivskyy, O.V. Ivanov, V.O. Moskaliuk, N.K. Shvachko, V.V. Zaika, S.S. Smolyak, *Appl. Phys. A* **132**, 430 (2026) https://doi.org/10.1007/s00339-026-09598-9.
37. S. Maniv, W.D. Westwood, E. Colombini, J. *Vac. Sci. Technol.* **20** No 2, 162 (1982) https://doi.org/10.1116/1.571350.
38. *Physics of Nonmetallic Thin Films* (Ed. by C.H.S. Dupuy, A. Cachard) (New York: Plenum Press: 1976).
39. G.D. Cody, T. Tiedje, B. Abeles, B. Brooks, Y. Goldstein, *Phys. Rev. Lett.* **47**, 1480 (1981) https://doi.org/10.1103/PhysRevLett.47.1480.
40. R.C. Rai, *J. Appl. Phys.* **113** No 15, 153508 (2013) https://doi.org/10.1063/1.4801900.

Вплив допування Bi на оптичні та структурні властивості тонких плівок ZnO: роль енергії Урбаха та механічних напружень

С.І. Шулима[1], Н.А. Курган[1], В.Х. Касіянeнко[2,1], В.Л. Карбівський[1], В.В. Стоніс[1], Н.О. Зуєва[1], О.А. Пузько[1], Л.П. Клюєнко[1], О.І. Соболєв[1]

[1] *Інститут металофізики ім. Г.В. Курдюмова НАН України, 03142 Київ, Україна*
[2] *Вінницький національний технічний університет, 21021 Вінниця, Україна*

Досліджено вплив концентрації допанта Bi на оптичні та структурні властивості тонких плівок ZnO, синтезованих методом радіочастотного магнетронного осадження, з фокусом на аналіз енергії Урбаха та внутрішніх механічних напружень. Показано, що підвищення концентрації Bi у плівках ZnO супроводжується зростанням механічних напружень, пов'язаних із локальними спотвореннями кристалічної гратки. Ці деформації можуть виникати внаслідок заміщення іонів Zn^{2+} більшими іонами Bi^{3+} або утворення вторинної фази Bi_2O_3, що в обох випадках спричиняє розвиток внутрішніх напружень у плівках. Встановлено, що при незначних концентраціях допанта Bi (до 1.8 ат. %) механічні напруження не впливають на діаметр наностовпчикової структури тонких плівок ZnO, тоді як при значних концентраціях (більше 5 ат. %) спостерігається пригнічення латерального росту наностовпчиків із відповідним зменшенням їх діаметрів. Показано, що енергія Урбаха допованих Bi плівок ZnO істотно перевищує відповідне значення для недопованих зразків, що вказує на розширення хвостів локалізованих станів у забороненій зоні внаслідок допування вісмутом. Хоча макроскопічні механічні напруження впливають на значення енергії Урбаха, її немонотонна залежність від концентрації Bi зумовлена насамперед іншими чинниками – зокрема локальними флуктуаціями електростатичного потенціалу та розорієнтацією наностовпчикової структури.

Ключові слова: Тонкі плівки ZnO, Радіочастотне магнетронне розпилення, Оптичні властивості, Структурні властивості, Енергія Урбаха, Механічні напруження.